Hydrol. Earth Syst. Sci., 27, 1243–1259, 2023
https://doi.org/10.5194/hess-27-1243-2023

Hydrology and Earth System Sciences
Open Access
EGU

Improving the understanding of N transport in a rural catchment under Atlantic climate conditions from the analysis of the concentration–discharge relationship derived from a high-frequency data set

María Luz Rodríguez-Blanco[1], María Teresa Taboada-Castro[2], and María Mercedes Taboada-Castro[3]

[1]Physical Geography Area, History, Art and Geography Department, GEAAT Group, University of Vigo, Campus As Lagoas, 36310 Ourense, Spain
[2]Faculty of Sciences, University of A Coruña, 15071 A Coruña, Spain
[3]ETSIIAA, Area of Soil Science and Soil Chemistry, University of Valladolid, 34004 Palencia, Spain

Correspondence: María Luz Rodríguez-Blanco (maria.luz.rodriguez.blanco@uvigo.es)

Received: 27 October 2021 – Discussion started: 30 November 2021
Revised: 3 December 2022 – Accepted: 28 February 2023 – Published: 21 March 2023

Abstract. Understanding processes controlling stream nutrient dynamics over time is crucial for implementing effective management strategies to prevent water quality degradation. In this respect, the study of the nutrient concentration–discharge (C–Q) relationship during individual runoff events can be a valuable tool for extrapolating the hydrochemical processes controlling nutrient fluxes in streams. This study investigated nitrogen concentration dynamics during events by analyzing and interpreting the nitrogen C–Q relationship in a small Atlantic (NW Iberian Peninsula) rural catchment. To this end, nitrate (NO_3-N) and total Kjeldahl nitrogen (TKN) concentrations were monitored at a high temporal resolution during 102 runoff events over a 6-year period. For each of the selected runoff events, C–Q response was examined visually for the presence and direction of hysteresis loops and classified into three types of responses, namely clockwise, counterclockwise, and no hysteresis. Changes in concentration (ΔC) and the hysteresis direction (ΔR) were used to quantify nitrogen (NO_3^- and TKN) patterns during the runoff events. The transport mechanisms varied between compounds. The most frequent hysteretic response for NO_3^- was counterclockwise with enrichment. On the contrary, the main TKN dynamic was enrichment with clockwise hysteresis. Event characteristics, such as rainfall amount, peak discharge (i.e., maximum discharge of the runoff event), and event magnitude relative to the initial baseflow (i.e., the difference between the maximum discharge of the runoff event and the initial baseflow divided by initial baseflow) provided a better explanation for hysteresis direction and magnitude for TKN than antecedent conditions (antecedent precipitation and baseflow at the beginning of the event). For NO_3^- hysteresis, the role of hydrometeorological conditions was more complex. The NO_3^- hysteresis magnitude was related to the magnitude of the event relative to the initial baseflow and the time elapsed since a preceding runoff event. These findings could be used as a reference for the development of N mitigation strategy in the region.

1 Introduction

Increasing nitrate concentrations in headwater catchments is a pressing environmental issue (EEA, 2018; Koenig et al., 2021; Musolff et al., 2021). In Europe, despite the advances made in the field of improving the quality of waterbodies in recent decades, 60 % of freshwater bodies fail to achieve good ecological status, as established by the Water Framework Directive (2000/60/EC; EEA, 2018). The European Union directive urges member states to monitor water quality. However, many of these countries, Spain among them, have an inadequate water monitoring network to ensure the comprehensive and consistent monitoring of waterbodies (EC, 2019). Historically, water quality assessments

have relied on routine low-frequency monitoring at main rivers, commonly at a biweekly or monthly resolution. This traditional sampling method can provide valuable information to identify sites that are under pressure due to anthropogenic activities, and also to observe long-term trends in relation to land use, but cannot provide knowledge on nutrient dynamics under contrasting hydrological conditions (Dupas et al., 2016; Rose et al., 2018; Musolff et al., 2021), which is essential to develop suitable management programs to restore or maintain water quality (Lloyd et al., 2016; Bieroza et al., 2018).

One way of approaching the study of these dynamics requires a high-frequency analysis of the nutrient concentration and discharge (C–Q) relationship at a given point in the stream during runoff events (Bieroza and Heathwaite, 2015; Lloyd et al., 2016; Rose et al., 2018; Baker and Showers, 2019). The hysteresis loop is the most typical pattern observed in the nutrient C–Q relationship (Evans and Davies, 1998). It reflects a nonlinear nutrient concentration behavior because the concentration at a given discharge on the rising limb differs from that of the same discharge on the falling limb of the hydrograph (Evans and Davies, 1998). The width, magnitude, and direction of these loops have been used to investigate the sources, flow paths, and transport mechanisms responsible for the export of nutrients from catchments (Evans and Davies, 1998; Butturini et al., 2008; Dupas et al., 2016; Vaughan et al., 2017; Barros et al., 2020). Hysteresis C–Q relationships can be classified into clockwise and counterclockwise according to their direction (Fig. 1). Clockwise hysteresis is generally understood to reflect proximal and rapidly mobilized sources, whereas counterclockwise hysteresis reflects sources that are either proximal to the stream channel with slow transport or those that are distant to the stream (Williams, 1989; Evans and Davies, 1998; Lloyd et al., 2016; Baker and Showers, 2019; Knapp et al., 2020). Complex hysteresis loops are often the result of the spatiotemporal variability in rainfall and antecedent moisture conditions (Ramos et al., 2015). The C–Q relationship can also result in positive or negative hysteresis slopes representing enrichment or dilution effects, respectively (Butturini et al., 2008; Lloyd et al., 2016; Vaughan et al., 2017).

Numerous studies have examined the nitrogen species, particularly nitrate (NO_3^-), and the C–Q relationship at the event scale in varying sizes of catchments under different degrees of human impact (e.g., Butturini et al., 2008; Cerro et al., 2014; Dupas et al., 2016; Outram et al., 2016; Vaughan et al., 2017; Baker and Showers, 2019; Musolff et al., 2021; Winter et al., 2021), showing evidence of diverging C–Q relationships in agricultural and forest catchments. For example, in intense agricultural management, the catchment NO_3^- showed a consistent response between events that was dominated by clockwise enrichment or dilution patterns (Cerro et al., 2014; Dupas et al., 2016; Outram et al., 2016). In the case of forested catchments, where the NO_3^- response was highly variable, a NO_3^- enrichment C–Q pattern with a clockwise or counterclockwise hysteresis was prevalent (Vaughan et al., 2017; Musolff et al., 2021). Hysteresis patterns can change from one runoff event to another, and several factors, such as antecedent wetness conditions, rainfall depth, and runoff volume, as well as event water contributions, play an important role in controlling the variability in the NO_3^- C–Q relationship among various hydrological events (Outram et al., 2016; Baker and Showers, 2019; Knapp et al., 2020). For example, Knapp et al. (2020) observed dilution behavior during wetter conditions and stronger mobilization following drier ones and during events with larger event water contributions. However, others found that NO_3^- hysteresis behavior was better explained by the runoff event magnitude and rainfall intensity (Butturini et al., 2008; Aguilera and Melack, 2018). Comparatively, approaches for the analysis of the organic N C–Q relationships at the event scale are scarce when the focus is mostly on organic dissolved nitrogen (e.g., Kaushal and Lewis, 2003; Chen et al., 2012; D'Amario et al., 2021). The literature suggests that, even though dissolved organic nitrogen accounts for only part of the nitrogen in streams draining in agricultural management catchments, both particulate and dissolved forms of organic nitrogen can constitute a substantial quantity of the total nitrogen export in rural and forested catchments (Hagedorn et al., 2000; Kaushal and Lewis, 2003; Aguilera and Melack, 2018). Thus, Lorite-Herrera et al. (2009) pointed out that dissolved organic nitrogen is the dominant form of nitrogen in an intensively farmed catchment in southeastern Spain (72 %–97 %). Similarly, Hagedorn et al. (2000) and Kaushal and Lewis (2003) found that organic nitrogen accounted for approximately 60 % of total annual nitrogen in their study areas in the Erlenbach headwaters basin (Switzerland) and the Rocky streams (Canada). Bernal et al. (2005), on the other hand, reported a moderate fraction (35 %) of the N annual flux in the form of dissolved organic nitrogen in a Mediterranean forested catchment in Catalonia (NE Spain), while Rodríguez-Blanco et al. (2015) reported a more than 25 % contribution of total Kjeldahl nitrogen (TKN) to total nitrogen in a rural catchment in NW Spain. Therefore, the analysis of NO_3^- and total organic nitrogen C–Q relationships may provide useful information about the processes regulating N transport through the landscape. So far, there are few studies integrating both NO_3^- and total organic nitrogen C–Q relationships into a coherent framework in the southwest of Europe, partly due to the limited availability of high-frequency data. This information is essential in order to anticipate changes in the quality of freshwater resources in compliance with the Water Framework Directive planning and monitoring norms. Therefore, it is necessary to provide new information on the issue to augment current studies across Europe and the Iberian Peninsula, in particular.

In this context, the aim of this study was to understand differences in the behavior of NO_3^- and TKN concentrations. For this, we used high-frequency measurements of NO_3^-

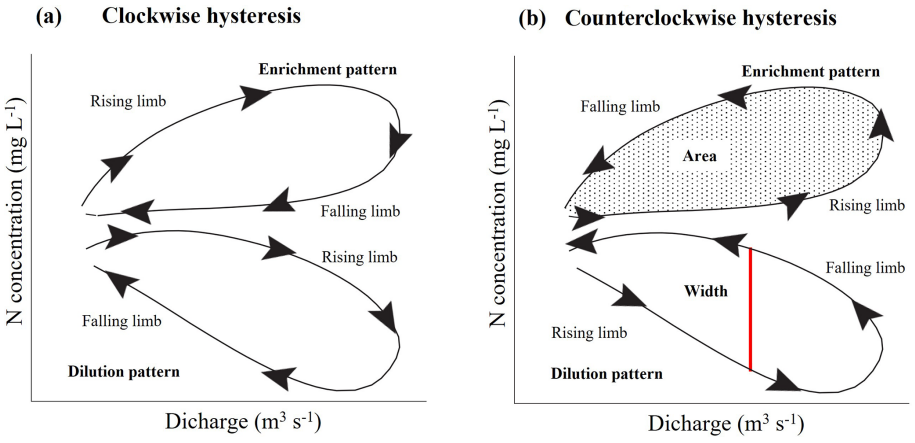

Figure 1. Idealized representation of **(a)** clockwise and **(b)** counterclockwise hysteresis loops, showing that each pattern can occur with either enrichment or dilution during the rising limb of the hydrograph. The loop width (size of the loop; i.e., the difference in concentration between the rising and falling limbs at the midpoint of discharge) and area are shown in panel **(b)**.

(expressed as NO_3-N) and the TKN concentration obtained during runoff events of contrasting magnitudes at the outlet of an Atlantic headwater catchment located in the NW Iberian Peninsula. More specifically, the study aims to explore questions such as (i) how NO_3^- C–Q behavior differs from that of TKN C–Q, (ii) how variable C–Q relationships between individual events are, and (iii) whether variability in C–Q relationships can be explained by specific rainfall–runoff event characteristics, such as antecedent wetness conditions, rainfall, runoff volume, etc. The selected catchment (Corbeira; 16 km^2l NW Iberian Peninsula) is of particular interest, as it is a tributary of Río Mero, which discharges into the Abegondo–Cecebre reservoir – the main water supply for the city of A Coruña and surrounding municipalities (450 000 inhabitants) – and finally drains into the Atlantic Ocean through the Ria de O Burgo. The Abegondo–Cecebre reservoir is a Natura 2000 EU site, classified as a Special Area of Conservation (ES1110004) in 2014 under the EU Habitats Directive (92/43/ECC) and one of the core zones of the Mariñas Coruñesas e Terras do Mandeo Biosphere Reserve, sustaining important bird, macroinvertebrate, and fish populations. Nevertheless, the ecological status of the Abegondo–Cecebre reservoir has deteriorated in the last few decades due to pollution, the presence of invasive alien species, and fluctuations in river flow discharge (Ameijenda, 2010).

2 Material and methods

2.1 Study site

The study was conducted in a headwater catchment of 16 km^2 located in NW Spain, approximately 30 km southeast of the city of A Coruña (Galicia, NW Iberian Peninsula; Fig. 2). The catchment is characterized by low drainage density (1.38 km km^{-2}), a mean slope of 19 %, and a maximum altimetric amplitude of 410 m (65–675 m). The bedrock consists of basic schist of the Órdenes Complex (IGME, 1981), and the soils are dominantly Umbrisols and Cambisols (IUSS, 2015), with a silt and silty loam texture, variable organic matter content (4.4 %–10.5 %), and acid pH in the surface soil layer. The soils have a high infiltration capacity, so overland flow is unusual. Groundwater is the dominant source of water to the stream, and the baseflow index is 0.75 (Rodríguez-Blanco et al., 2012). The catchment land cover comprises a mixture of forest (65 %), agricultural fields (30 %), and impervious areas (5 %), consisting of roads and single-family homes that are not always connected to sewage disposal systems. Agricultural areas are dominated by pastures (26 % of the total area), and the remaining fields (4 %) grow maize and winter cereals. Organic and inorganic fertilizers are commonly used in agricultural areas throughout the year, including the wettest months. Forest areas are not fertilized. The annual N input to the Corbeira catchment is approximately 37.8 kg N ha^{-1} (Rodríguez-Blanco et al., 2015), indicating relatively low nitrogen inputs in the Corbeira catchment compared to catchments with more intensive agriculture.

The study area is located within the Eurosiberian biogeographic region, particularly in the Cantabrian–Atlantic province (Instituto Geográfico Nacional, 2008). It is included in the temperate oceanic climate region (Csb), according to the Köppen–Geiger classification. Mean annual rainfall and temperature for the period 1983–2020 are 1075 mm and 13 °C, respectively (data from the station ID 10045 of the official meteorological service of the Galician government (MeteoGalicia), located approximately 8 km from the catchment outlet). The wettest period is from October–March, and the driest and hottest months are usually in summer (June–September). The hydrological regime is pluvial oceanic, with

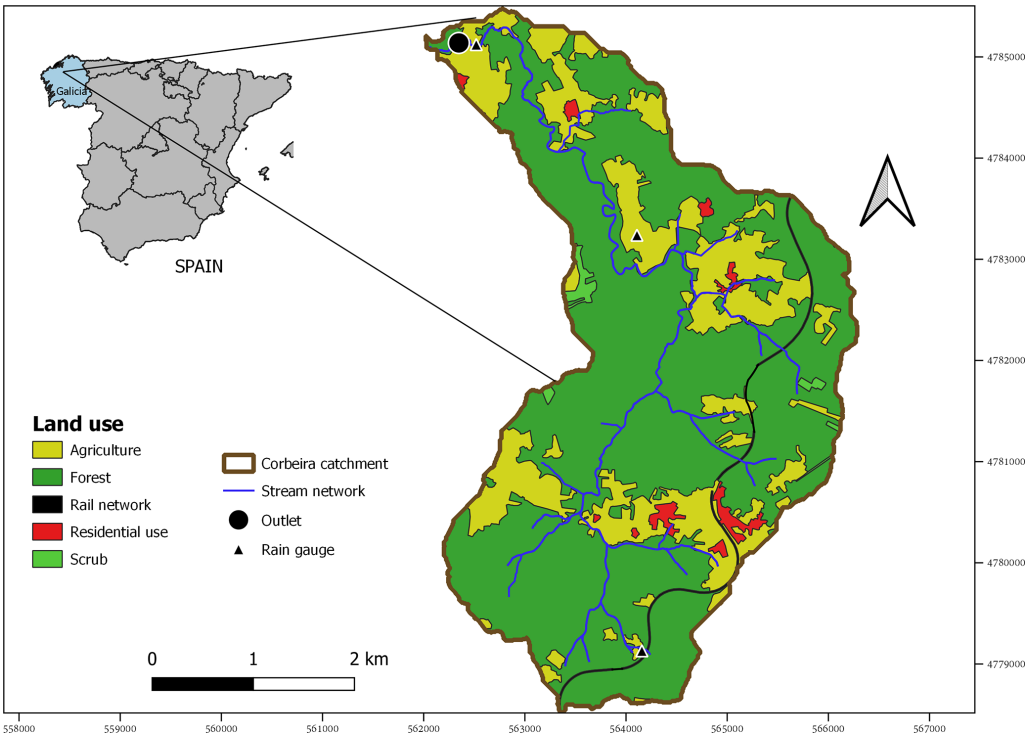

Figure 2. Location and land use of the Corbeira catchment.

maximum discharge in December and low flows from June–September. Mean daily recorded discharge is 0.18 $m^3 s^{-1}$. For more detailed information of the hydrological behavior of this catchment, see Rodríguez-Blanco et al. (2012, 2020).

2.2 Data acquisition: monitoring, sampling, and water analysis

The research period comprised 6 hydrological years (1 October–30 September) during which rainfall, discharge, and N (NO_3^- and TKN) concentrations were measured. Rainfall was monitored at 10 min intervals using three gauges (0.2 mm resolution) distributed across the catchment. The Thiessen polygon method (Linsey et al., 1949) was used to calculate the mean rainfall in the catchment. Water discharge was obtained at 10 min resolution at the catchment outlet. Stream water level was measured with a differential pressure transducer sensor (ISCO 720) coupled to an automatic water sampler (ISCO 6712 Full Size) at 1 min intervals and recorded at 10 min resolution. The water level was then converted into discharge by a rating curve development over a wide range of discharge conditions at the sampling location.

Stream water samples were taken at the catchment outlet during runoff events using the automatic water sampler (Teledyne ISCO; 6712 Full Size) fitted with 24 polypropylene 1 L bottles. The pump inlet of the autosampler was placed near the pressure sensor. In order to characterize the dynamics of N concentrations from the onset of runoff events, the sampler was configured to start collecting water samples when the stream water level rose by 2–3 cm above that at the beginning of a rainfall event. The criteria established by Dunkerley (2008; i.e., considering the minimum inter-event time and the minimum rainfall depth) have been used to define rainfall events. In this assessment, a single rainfall event was defined for a minimum rainfall depth of 5 mm (not interrupted by gaps of more than 1 h) and a minimum inter-event time of 10 h. The end of a rainfall event was determined by the last non-zero rainfall pulse. The choice of these thresholds to define a single rainfall event is due to fact that the hydrological response to less than 5 mm of rain volume is practically undetectable in the study area (Rodríguez-Blanco et al., 2012; Palleiro et al., 2014). In addition, the 10 h inter-event period (4.5 h – a value of more than double the concentration time of the catchment; Rodríguez-Blanco et al., 2012) was selected to ensure that the hydrological response of the catchment to individual rainfall events did not overlap between events.

Water samples were taken at fixed intervals (1–8 h) during the rising and falling limbs of the hydrograph to collect key runoff phases. The pumping frequency was modified manually, depending on the expected magnitude and duration of runoff events, based on weather forecasts together with the experience accumulated from water sampling over the years. Samples were removed from the autosampler within a few hours after runoff events and transported to the laboratory,

where they were stored in the dark and refrigerated at 4 °C until the total Kjeldahl nitrogen (TKN) and nitrate (expressed as NO_3-N) concentrations were analyzed. TKN concentrations were determined by the Kjeldahl digestion of unfiltered samples, following the American Public Health Association method (APHA, 1998), whereas NO_3^- concentrations were analyzed by capillary electrophoresis after sample filtration (0.45 µm).

2.3 Selection of runoff events and description of $C-Q$ hysteresis

In this study, the runoff events were identified as any hydrological response to rainfall in which the discharge increased by an amount at least 1.5 times that recorded at the beginning of the event (Tardy, 1986; García-Ruiz et al., 2005). For each runoff event, the stream discharge was separated into two components (direct runoff and baseflow), using the constant slope hydrograph separation method by Hewlett and Hibbert (1967) and a constant slope of $1.83\,L\,s^{-1}\,km^{-2}\,d^{-1}$, as suggested in other Spanish forested catchments (e.g., Latron et al., 2008). The starting point of the runoff event has been identified as being a sudden increase in discharge in response to a rainfall, meaning that stream discharge increases by at least 5 % in a 30 min interval (three time steps). The end of the event was fixed at the point at which the direct runoff ended (i.e., the time when the constant slope line used in the separation of runoff components intersects the falling limb of the hydrograph; Fig. 3) or when a different hydrological event, identified by another increase in stream discharge (at least 5 % in three time steps) following the associated rainfall, commenced. In the latter case, the limit between runoff events was defined as the minimum discharge recorded between them.

The potential mechanism and processes controlling the hysteresis dynamics can be represented and quantified by potential explanatory variables that may explain the variability in hysteresis (Fovet et al., 2018). Two categories of potential explanatory variables can be considered, namely catchment characteristic (slope, soil type, and land use) and event-scale hydrobiogeochemical variables. Within the same catchment, the variability in the hysteresis patterns is highly influenced by event-scale properties ranging from hydrological, biogeochemical, and antecedent conditions (Butturini et al., 2006; Outram et al., 2016; Aguilera and Melack, 2018; Heathwaite and Bieroza, 2020). In order to study the influence of different event-scale hydrobiogeochemical variables on the hysteresis dynamics of NO_3^- and TKN, the events were characterized by three groups of variables, including (i) those related to antecedent wetness conditions (i.e., variables characterizing the conditions prior to the event), (ii) event variables (rainfall and discharge), and (iii) variables related to NO_3^- and TKN concentrations (Table 1) as the nitrogen dynamic (response variables and hysteresis descriptors). Antecedent wetness conditions were described by accumulated rainfall 7 and 15 d prior to the event (AP7d and AP15d, respectively; mm), the discharge at the beginning of the event (Q_b; $m^3\,s^{-1}$), and the time elapsed from the previous runoff event (Δt; h). Event variables included the following:

- rainfall amount (P; mm);
- maximum 10 min rainfall intensity (IP10; $mm\,h^{-1}$);
- rainfall kinetic energy (KE; $MJ\,ha^{-1}$), determined according to Wischmeier and Smith (1958);
- peak discharge (Q_{max}; $m^3\,s^{-1}$);
- total runoff (TR; mm), i.e., total water volume during the runoff event (direct runoff + baseflow);
- magnitude of the event relative to the initial baseflow (ΔQ), i.e., $(Q_{max} - Q_b)/Q_b \times 100$; %);
- relative length of the rising limb (RL; %), given by $RL = R_D/S_D \times 100$, where R_D and S_D are the length (h) of the rising limb of the hydrograph (i.e., the part of a hydrograph from the start of the runoff event to the peak discharge) and of the entire hydrograph (runoff event duration; i.e., the time difference in hours between the start and finish), respectively; and
- slope of the initial phase (2 h) of the hydrograph falling limb (i.e., the part of the hydrograph from peak discharge to the end of the runoff event) estimated using an exponential model (Singh, 1988) (K, $1\,d^{-1}$).

Finally, to describe NO_3^- (NO_3-N) and TKN concentrations, the initial, maximum, and discharge-weighted mean concentrations of NO_3^- and TKN measured during the events were included (NO_3-$NC_{initial}$, NO_3-NC_{max}, NO_3-NC_{mean}, $TKNC_{initial}$, $TKNC_{max}$, and $TKNC_{mean}$, respectively; $mg\,L^{-1}$). The discharge-weighted mean concentration of the event was computed as the total load divided by the total flow.

During the entire monitoring period, 173 runoff events were identified; 156 were sampled, and the other 17 were missed because of technical problems with the equipment. In this assessment, the only events used were those with a single peak discharge and at least two samples collected on each limb of the hydrograph, with one at or close to the peak discharge (30 min). This was the minimum needed to identify the rotational direction (Evans and Davies, 1998), and the rest were discarded. By applying these criteria, only 102 of the 156 events sampled were included in the $C-Q$.

For each of the selected runoff events, the $C-Q$ NO_3^- and TKN response was evaluated visually for the presence and direction of a hysteresis loop (by plotting concentration versus discharge) and grouped into three types of responses, namely clockwise, counterclockwise, and no hysteresis. Events with a figure-eight hysteresis pattern were

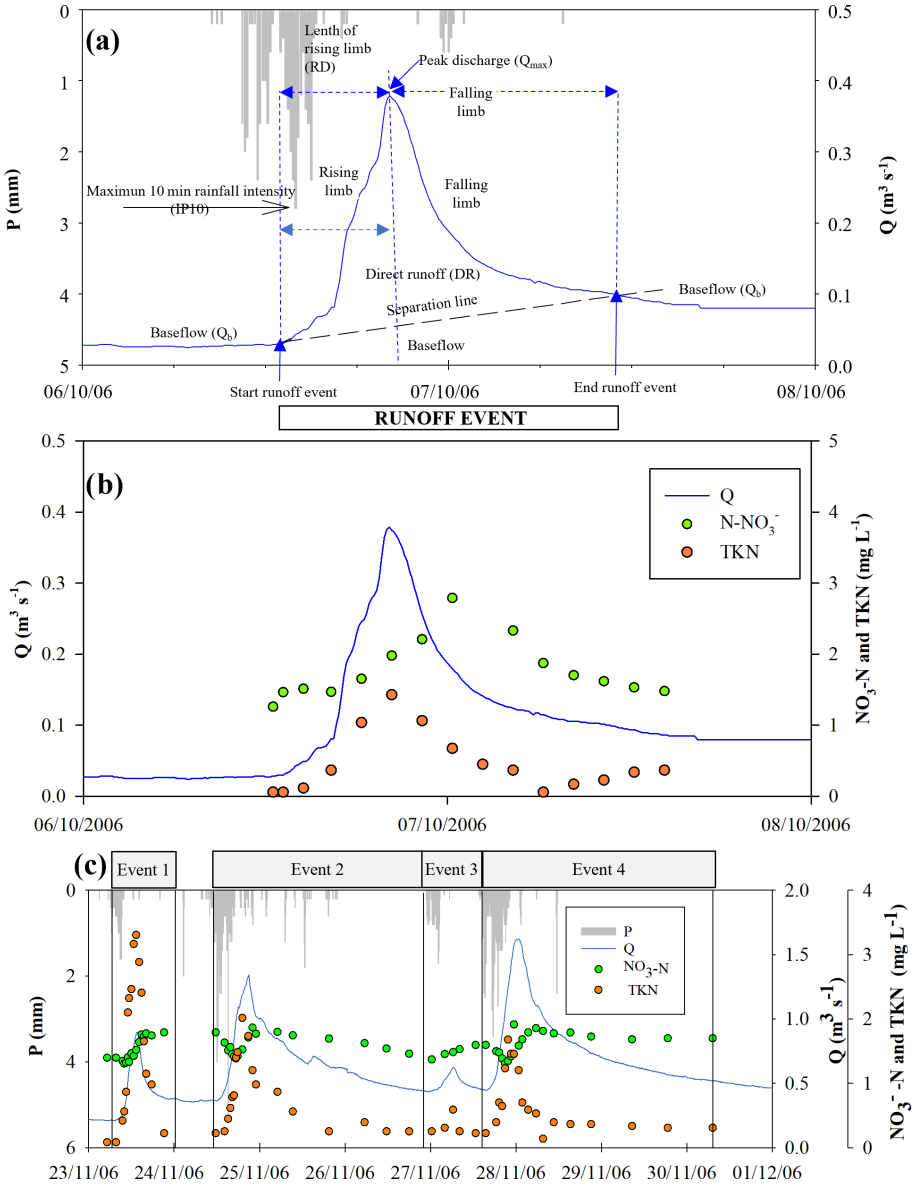

Figure 3. **(a)** Diagram illustrating the hydrograph separation in two components (direct runoff and baseflow), using the constant slope hydrograph separation by Hewlett and Hibbert (1967). Some variable characteristics of the rainfall–runoff events are also indicated. **(b)** Example of evolution of NO_3^- (NO_3-N) and TKN concentrations during a runoff event. **(c)** Sequence of rainfall–runoff events and evolution of NO_3^- (NO_3-N) and TKN concentrations.

classed as a hysteresis response, with the direction depending on the succession of the peak concentration and peak discharge (i.e., clockwise or counterclockwise), similar to Bieroza and Heathwaite (2015).

Following the methodology proposed by Butturini et al. (2008), the form, rotational patterns, and slope of the NO_3^- and TKN hysteresis loops were characterized by two descriptors, namely hysteresis magnitude (ΔC; %) and hysteresis direction (ΔR, %). Hysteresis magnitude (ΔC) describes the relative changes in nitrogen (NO_3^- or TKN) concentration and hysteresis slope and is calculated using the following:

$$\Delta C \begin{cases} \frac{C_s - C_b}{C_{max}} \cdot 100 & \text{if } C_s > C_b \\ \frac{C_s - C_b}{C_b} \cdot 100 & \text{if } C_s < C_b \end{cases}, \quad (1)$$

where C_s and C_b are the nitrogen (NO_3^- or TKN) concentrations at peak discharge and baseflow, respectively, and C_{max} is the highest concentration measured in the stream during the runoff event. ΔC ranges from -100 % to 100 %, where positive values indicate hysteresis loops following a positive slope with respect to the discharge (i.e., element flushing)

Table 1. Characteristics of the runoff events ($n = 102$) selected during the study. CV is the coefficient of variation.

Variable		Mean	Minimum	Maximum	CV (%)
Antecedent conditions	Accumulated rainfall 7 d before the event (AP7d; mm)	35.18	0.60	124.40	81
	Accumulated rainfall 15 d before the event (AP15d; mm)	67.29	1.00	222.10	77
	Discharge at the beginning of the event (Q_b; $m^3 s^{-1}$)	0.21	0.03	0.64	60
	Time from the previous runoff event (Δt; h)	236.83	0.00	4065.02	212
Event conditions	Rainfall amount (P; mm)	22.24	5.00	74.40	69
	Maximum 10 min rainfall intensity (IP10; $mm h^{-1}$)	2.35	0.40	9.20	71
	Rainfall kinetic energy (KE; $MJ ha^{-1}$)	3.16	0.52	10.49	74
	Peak discharge (Q_{max}; $m^3 s^{-1}$)	0.49	0.10	1.62	65
	Total runoff volume (TR; mm)	2.54	0.26	1.88	99
	Magnitude of the event relative to initial baseflow (ΔQ; %)	165.57	17.65	853.33	92
	Relative length of the rising limb (RL; %)	33.63	11.63	64.35	38
	Slope of the initial phase of the hydrograph falling limb (K; $1 d^{-1}$)	−0.016	−0.053	−0.001	72
	Runoff event duration (S_D; h)	32.41	9.80	115.80	59
NO_3 and TKN concentrations during the events	NO_3^-				
	Initial concentration (NO_3-$NC_{initial}$; $mg L^{-1}$)	1.22	0.70	2.84	27
	Maximum concentration (NO_3-NC_{max}; $mg L^{-1}$)	1.60	0.71	5.09	41
	Mean concentration (NO_3-NC_{mean}; $mg L^{-1}$)	1.31	0.70	2.27	25
	TKN				
	Initial concentration ($TKNC_{initial}$; $mg L^{-1}$)	0.25	0.01	2.55	129
	Maximum concentration ($TKNC_{max}$; $mg L^{-1}$)	1.47	0.08	9.41	96
	Mean concentration ($TKNC_{mean}$; $mg L^{-1}$)	0.6375	0.04	2.88	79
Hysteresis descriptors	NO_3^-				
	Hysteresis direction (ΔR; %)	−20.62	−93.00	60.00	151
	Hysteresis magnitude (ΔC; %)	3.86	−44.28	47.20	395
	TKN				
	Hysteresis direction (ΔR; %)	4.78	−72.00	69.00	513
	Hysteresis magnitude (ΔC; %)	66.15	−70.35	98.45	61

and negative values indicate the opposite (i.e., solute dilution). Hysteresis direction (ΔR) reflects the entire element dynamics during runoff events and provides information on the area (magnitude) and rotational (direction) pattern of the C–Q hysteresis. ΔR is calculated by the following:

$$\Delta R = R \cdot \mathrm{Ah} \cdot 100, \quad (2)$$

where Ah is the area of the C–Q hysteresis, estimated after standardizing the discharges and concentrations to the unit dividing nitrogen (NO_3^- or TKN) concentrations and discharge by their peak values and calculating the area under the loop. Thus, Ah takes values between 0 and 1; as the Ah value approaches zero, the loop becomes more linear, indicating minor differences in nitrogen (NO_3^- or TKN) concentrations between the rising and falling limbs. On the contrary, an Ah value close to 1 indicates that the area of the hysteresis loop is large, showing strong differences in nitrogen (NO_3^- or TKN) concentrations in both limbs of the hydrograph at similar discharge. R describes the rotational pattern of the hysteresis. If the C–Q hysteresis is clockwise, then $R = 1$, and if it is counterclockwise, then $R = -1$; for ambiguous or nonexistent hysteresis, $R = 0$. The descriptor ΔR also varies from −100 % to 100 %.

The variability in NO_3^- and TKN hysteresis descriptors was examined by plotting hysteresis magnitude (ΔC) versus the hysteresis direction (ΔR). The plots can be divided in four zones (Butturini et al., 2006), each of which identifies a C–Q response type (Fig. 4). For this, ΔC and ΔR descriptors were divided into two categories (−1; 1), namely $\Delta C < 0$ (element dilution) and $\Delta C > 0$ (element release), together with $\Delta R < 0$ (counterclockwise loop) and $\Delta R > 0$ (clockwise loop).

2.4 Statistical methods

To assess the main links between hysteresis descriptors (response variables) and the different hydrometeorological and biogeochemical (i.e., NO_3 and TKN concentrations) variables (explanatory variables), standard statistical methods were used, such as correlation (Pearson correlation coefficient) and a redundancy analysis (RDA). A Pearson correlation analysis provides a quantitative estimation of the degree of linear correlation between hydrometeorological and

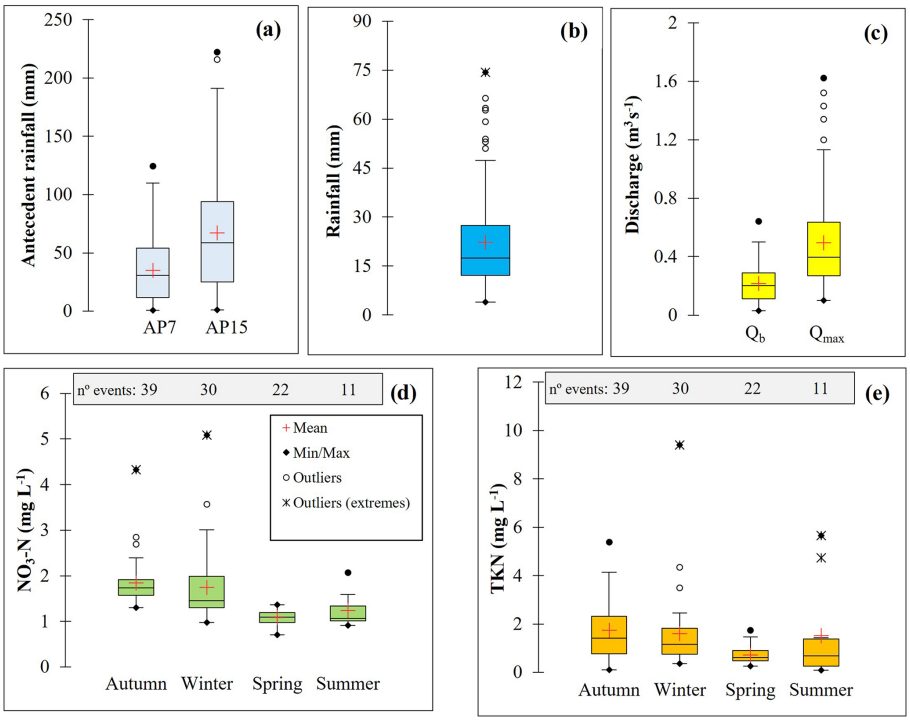

Figure 4. Box plot summarizing the characteristics of the events. **(a)** Antecedent rainfall. **(b)** Rainfall amount. **(c)** Discharge. **(d)** NO_3 concentrations (NO_3-N). **(e)** TKN concentrations. The box shows the interquartile range (IQR), which is defined as the difference between the third and the first quartile. The horizontal line within the box shows the median. The whiskers shown the 1.5 times IQR beyond the box. The outliers are values between 1.5 and 3 times the IQR, which is larger than third quartile, or values between 1.5 and 3 times the IQR, which is lower than the first quartile. The extreme outliers show values 3 times the IQR, which is larger than third quartile, or 3 times the IQR, which is lower than the first quartile.

biogeochemical variables with hysteresis descriptors. The RDA was used to investigate the multivariate relationship between response variables (hysteresis descriptors) and explanatory variables (hydrometeorological and biogeochemical variables). The RDA is an extension of the principal component analysis to data sets in which there are multiple response variables modeling the effects of explanatory variables on response variables assuming linear relationships; thus, it enables an examination of the variation in a matrix of variables (hysteresis descriptors) that can be explained by a matrix of predictor/explanatory variables (hydrometeorological and biogeochemical variables; Legendre and Legendre, 1998). Moreover, RDA can be used when variables cannot be considered strictly independent from each other, as in this case (ΔC and ΔR), where both descriptors are undoubtedly related. The RDA output was represented in a biplot graph showing the correlation between explanatory and response variables given by the cosine of the angle between vectors. Thus, vectors pointing in roughly the same direction represent a positive correlation, those pointing in opposite directions show a negative correlation, and vectors crossing at right angles indicate a near-zero correlation.

3 Results

3.1 Average characteristics of the rainfall–runoff events

The main characteristics of the selected events for this study are summarized in Table 1 and Fig. 4. High variability in the variables defining the events was observed. Thus, the events varied greatly in terms of antecedent conditions (AP7d is 0.60–124.40 mm, AP15d is 1.00–222.10 mm, and Q_b is 0.03–0.64 $m^3 s^{-1}$), meteorological (P is 4.00–74.40 mm, and KE is 0.52–10.49 MJ ha^{-1}) and hydrological features (Q_{max} is 0.10–1.62 $m^3 s^{-1}$, ΔQ is 17.65 %–853.33 %, and S_D is 9.80–115.80 h), showing that those selected cover a wide range of meteorological and hydrological conditions. These events (i.e., the 102 used in the study) can be considered representative of the rainfall–runoff event characteristics of the study period because the meteorological and hydrological data used in this study are within the 5th to 95th percentile range of rainfall, antecedent rainfall, and discharge of the events occurring in the area during the study period.

From the selected 102 rainfall–runoff events, 39 occurred in autumn (October–December), 30 in winter (January–March), 22 in spring (April–June), and 11 in summer (July–

September), so that about 70 % were concentrated in the wettest period of the year (October–March). The magnitude of the runoff events tended to be high in autumn and winter, when soil moisture is high, while in summer, when the catchment is drier, the event magnitude tended to be lower (Rodríguez-Blanco et al., 2012; Fig. 5c). In the study area, the runoff events are usually linked to low-volume (mean $P = 22.24$ mm) and intensity (mean IP10 $= 2.35\,\mathrm{mm\,h^{-1}}$) rainfall events of a long duration (mean = 14.8 h, min = 2 h, and max = 52.5 h), although several events with rainfall with a high volume ($P > 50$ mm) and intensity (IP10 $= 9.1\,\mathrm{mm\,h^{-1}}$) were registered during the study (Table 1). For most runoff events, an increase in NO_3-N and TKN concentrations with discharge were observed, but the magnitude of the increase varied markedly from one event to another. The mean and maximum N (NO_3-N and TKN) concentrations also varied among runoff events, especially for TKN; the maximum $TKNC_{mean}$ and $TKNC_{max}$ values were 2 orders of magnitude higher than the respective minimum values (Table 1). The highest values of both elements were recorded during autumn and winter events (Fig. 4).

3.2 Hysteresis direction and magnitude

The study of the relationship between the N (NO_3-N and TKN) concentration and discharge revealed different hysteresis patterns for both elements in the catchment (Figs. 5 and 6). For NO_3^-, the parameter describing the change in concentration during the runoff events returned positive values ($\Delta C \geq 0$ %) in 63 % of the events. These positive values show that NO_3-N concentrations during the runoff events were mostly greater than before the event; but 34 % had ΔC values between 0 % and 10 %, indicating a small increase in NO_3-N concentrations (Butturini et al., 2008). Based on hysteresis classification, 74 % of the events exhibited counterclockwise hysteresis ($\Delta R < 0$), 21 % clockwise hysteresis ($\Delta R > 0$), and the remaining 5 % showed no or unclear hysteresis patterns ($\Delta R = 0$). However, it should be noted that approximately 13 % of events returned ΔR values between −10 % and 10 %; therefore, the hysteresis area is considered to be small. NO_3^- data are in all areas in the ΔC vs. ΔR unit plane (Fig. 6 top), although the hysteresis loops are located mainly in zones D and C (Fig. 6 top), indicating dilution (negative ΔC) or flushing (positive ΔC) and counterclockwise hysteresis loops (negative ΔR).

TKN concentrations increased in almost all runoff events, when compared with pre-event values (positive ΔC in 93 % of events), indicating that TKN flushing clearly predominates over dilution. In fact, the parameter describing the change in the concentration during runoff events (ΔC) presented negative values in only 7 % of cases (Fig. 6; bottom), all of which were characterized by low rainfall. The rotational patterns of the TKN-Q hysteresis ranged from clockwise ($\Delta R > 0$) to counterclockwise ($\Delta R < 0$; Fig. 6; bottom). About 53 % of the events showed clockwise hysteresis, 39 % counterclockwise hysteresis, and the remaining 8 % showed no or unclear hysteresis patterns, although it should be noted that 29 % of the events showed small areas of the hysteresis loop (ΔR values stood between −10 % and 10 %). The hysteresis loops are located mainly in zones A and D (Fig. 6; bottom), suggesting a flushing (positive ΔC) and clockwise (positive ΔR) or counterclockwise loops (negative ΔR).

3.3 *C*–*Q* hysteresis response controls

The relationships between hysteresis descriptors and hydrological and biogeochemical variables were analyzed using a Pearson correlation matrix and an RDA analysis (Table 2 and Fig. 7) in order to identify the variables that might explain the C–Q hysteresis patterns. The results of the correlation analysis showed that the hysteresis direction and magnitude were more closely related to certain event characteristics than antecedent conditions (Table 2). Thus, of the representative variables of the event antecedent conditions, relevant correlations (negative sign) were observed between the discharge at the beginning of the event (Q_b) and the time from the previous runoff event (Δt) compared to the hysteresis magnitude parameter for NO_3 ($r = -0.22$, $p < 0.05$). The parameter describing information on the hysteresis direction for NO_3 (ΔR_{NO_3}) showed negative correlations with the rainfall amount (P), maximum 10 min rainfall intensity (IP10), rainfall kinetic energy (KE), and peak discharge (Q_{max}). On the contrary, a positive relationship was found between the hysteresis direction for TKN (ΔR_{TKN}) and rainfall amount (P), rainfall kinetic energy (KE), peak discharge (Q_{max}), total runoff volume (TR), and runoff duration (S_D).

Regarding the parameters describing the concentration status of NO_3^- (ΔC_{NO_3}) and TKN (ΔC_{TKN}), a positive correlation was found among these parameters (ΔC_{NO_3} and ΔC_{TKN}) and the hydrometeorological variables of rainfall amount (P), rainfall kinetic energy (KE), and magnitude of the event relative to the initial baseflow (ΔQ). An inverse relationship was found between ΔC_{TKN} and the relative length of the rising limb (RL; $r = -0.23$; $p < 0.01$) and slope of the initial phase of the hydrograph falling limb (K; $r = -0.31$; $p < 0.01$). Finally, the concentrations during runoff events were not controlling factors for the direction of the hysteresis of NO_3 and TKN, but these variables (especially $C_{initial}$) controlled the hysteresis magnitude for NO_3^- (ΔC_{NO_3}) and TKN (ΔC_{TKN}), although in different ways (Table 2). Thus, $C_{initial}$ showed positive correlations with ΔC_{NO_3} and negative with ΔC_{TKN}.

RDA analysis confirmed the Pearson's correlation results. The first two axes explained 70.1 % of the total variance in the descriptors in the NO_3^- and TKN hysteresis (ΔC_{NO_3}, ΔC_{TKN}, ΔR_{NO_3}, and ΔR_{TKN}), accounting for the first and second canonical axes for 45.8 % and 24.3 %, respectively. ΔC_{TKN} and ΔR_{TKN} loaded positively in the first axis and pointed in the same direction as rainfall–runoff magnitude variables; i.e., the rainfall amount (P), rainfall kinetic energy

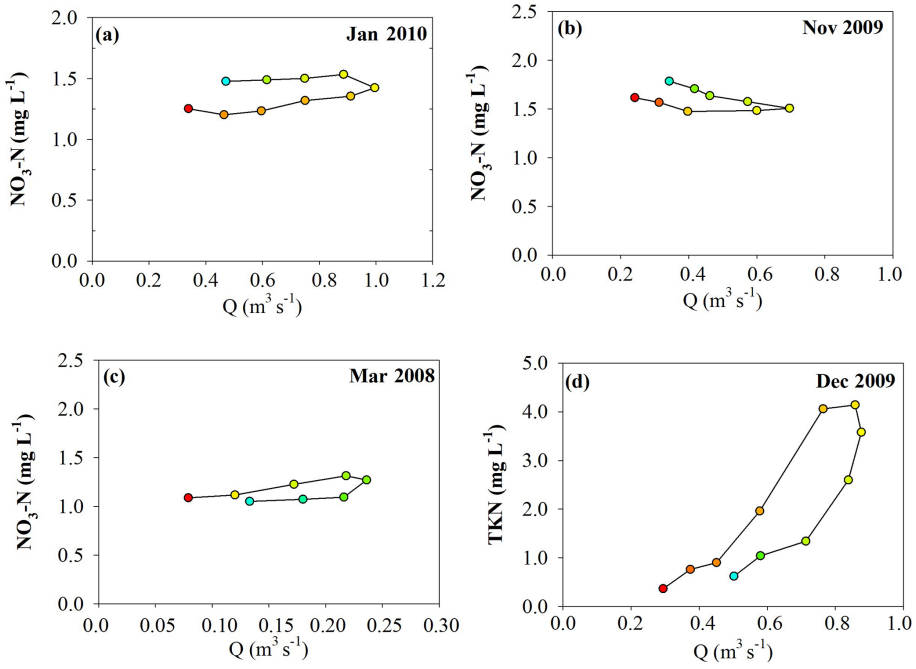

Figure 5. Examples of different types of NO_3^- **(a–c)** and TKN **(d)** hysteresis patterns observed in the Corbeira catchment during the monitoring period, where red indicates the start and blue the end of the runoff events. **(a)** Enrichment with a counterclockwise pattern. **(b)** Dilution with a counterclockwise pattern. **(c, d)** Enrichment with a clockwise pattern.

(KE), magnitude of the event relative to the initial baseflow (ΔQ), peak discharge (Q_{max}), and total runoff volume (TR), thus indicating a positive relationship with these. ΔR_{TKN} and ΔC_{NO_3} loaded negatively in the second axis and pointed in an opposite direction to the slope of the initial phase of the falling limb (K), suggesting that an inverse relationship exists between both variables. On the other hand, ΔR_{NO_3} loaded negatively in the first axis and pointed in the opposite direction to rainfall amount (P), rainfall kinetic energy (KE), magnitude of the event relative to the initial baseflow (ΔQ), and peak discharge (Q_{max}), indicating that an inverse relationship occurs with these variables.

4 Discussion

High-frequency water quality monitoring facilitates the identification of $C-Q$ dynamics at the event scale (Lloyd et al., 2016; Vaughan et al., 2017; Rose et al., 2018; Musolff et al., 2021; Winter et al., 2021). We observed that, in general, the NO_3-N and TKN concentrations increased during runoff events in comparison to pre-event conditions, indicating the predominance of an enrichment response during runoff events and suggesting that the N delivery in the catchment is mainly controlled by diffuse sources. Nitrate concentrations in drinking water in Europe are restricted to 50 mg L^{-1}, as NO_3^- or 11.3 mg L^{-1} NO_3^--N (EU Directive 98/83/EC), and this limit was not exceeded for the Corbeira catchment. However, considering that, in well-oxygenated surface waters, nitrate levels above 0.5–1.0 mg L^{-1} (as NO_3^-) can pose a risk of water eutrophication (Camargo and Alonso, 2007) and that 2 mg L^{-1} (as NO_3^-) is the threshold identified in the *European Nitrogen Assessment* as an appropriate target for establishing a river system in good ecological conditions, the data obtained (Table 1) indicate that the study area may be threatened by a potential risk of eutrophication due to the increased nitrogen concentration during individual events. It is also important to consider organic nitrogen (expressed as TKN), which accounts for a moderate fraction (> 25 %) of the total annual N export from the catchment (Rodríguez-Blanco et al., 2015) and can be a source of bioavailable nitrogen through the ammonification and subsequent nitrification of NH_4. All of this will clearly have important implications for compliance with water quality targets, and it must be borne in mind that the study area flows into the Abegondo–Cecebre reservoir, a very important source of drinking water for one of the largest cities in the northwestern Iberian Peninsula.

Nitrate and Kjeldahl nitrogen hysteresis patterns

The NO_3^- dynamic during the runoff events was dominated by counterclockwise hysteresis with enrichment. This pattern, in which higher concentrations are observed in the falling limb than the rising limb (Fig. 5a and b), is often the result of a greater subsurface flow contribution, followed by that of groundwater (Dupas et al., 2016; Rose et al., 2018; Musolff et al., 2021). Groundwater, which dominates base-

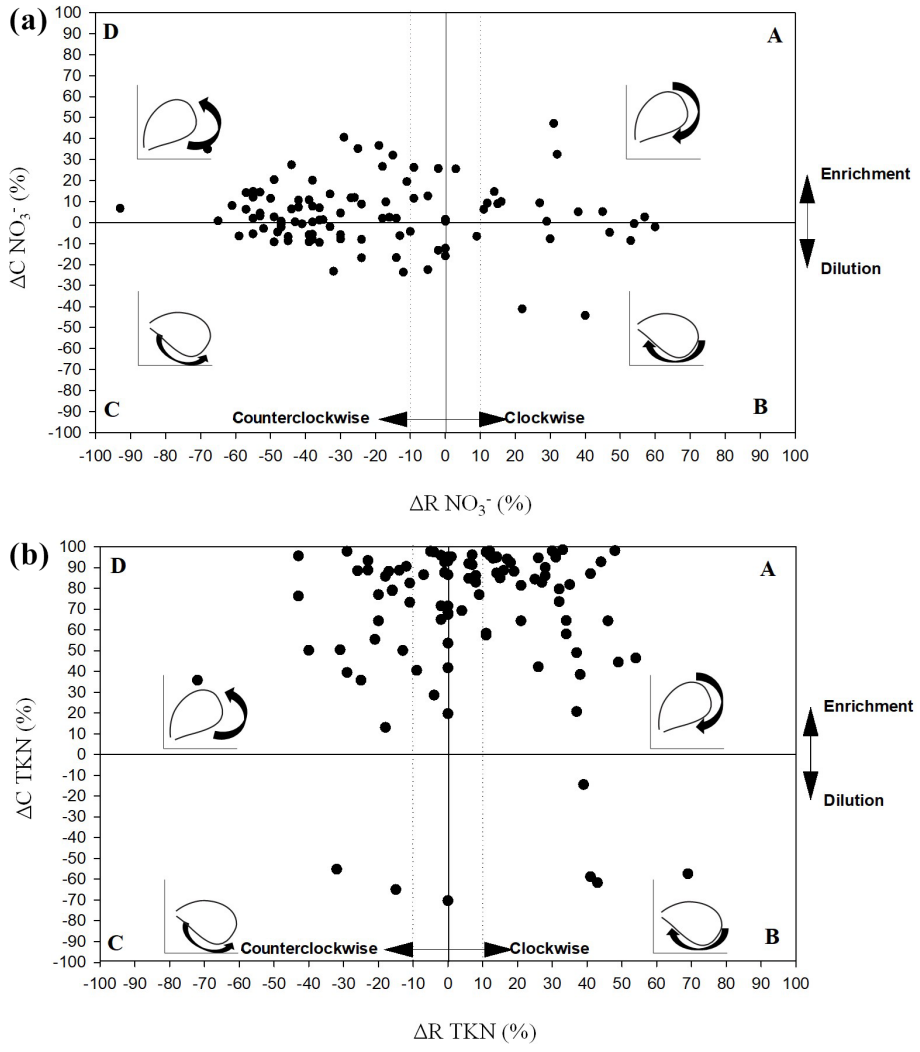

Figure 6. Representation of the C–Q hysteresis characteristics (ΔR and ΔC) of NO_3^- **(a)** and TKN **(b)** in the unity plane (A is the clockwise hysteresis with enrichment, B is the clockwise hysteresis with dilution, C is the counterclockwise hysteresis with dilution, and D is the counterclockwise hysteresis with enrichment). The vertical and horizontal dotted lines delimit the hysteresis loops with a small area. Circular arrows show the direction of clockwise and counterclockwise hysteresis (authors' own creation; based on Butturini et al., 2006).

flow, contains low NO_3^- concentrations in this catchment. Thus, Rodríguez-Blanco et al. (2015) showed that NO_3-N concentrations in summer (low-flow conditions dominated by groundwater) were lower (around 0.85 mg L^{-1}) than those measured in winter (1.28 mg L^{-1}). On the other hand, the soils in the study area have high infiltration rates (Taboada-Castro et al., 1999), and a great deal of streamflow comprises water leached through the soil profile (Rodríguez-Blanco et al., 2019), so subsurface flow is a likely pathway delivering additional NO_3^- during runoff events. Previous studies carried out in the catchment to make an approximate estimation of the contribution of surface flow and subsurface flow to direct runoff, using electrical conductivity as a tracer, have shown that subsurface flow constitutes the main route of generating direct runoff in the catchment (mean value of 72 %; 39 %–90 %; Rodríguez-Blanco, 2009). In addition, the largest contribution by the subsurface flow has been documented at the beginning of the falling limb (Rodríguez-Blanco, 2009), that is, when the highest NO_3 concentrations were recorded. This pattern (counterclockwise) could also be related to the higher availability of NO_3^- in the shallow soil horizon than in deeper groundwater, arguably because of the mineralization of organic matter and the mineral and organic fertilizer applied to agricultural soils in the catchment, as demonstrated by both modeling and data-driven approaches (López Periago et al., 2002). Other authors, however, have attributed counterclockwise hysteresis to a particular spatial distribution of the sources. Thus, Vaughan et al. (2017), in a study in a heavily fertilized agricultural catchment, linked this pattern to the transport of proximal sources at the begin-

Table 2. Pearson correlation coefficients between hysteresis descriptors (ΔR and ΔC) and event characteristics. Values displayed in bold indicate that the correlation is significant at the 0.01 level, and italics indicate that the correlation is significant at the 0.05 level.

	Hysteresis direction (ΔR)		Hysteresis magnitude (ΔC)	
	NO_3^-	TKN	NO_3^-	TKN
Antecedent conditions				
AP7d	−0.18	0.09	−0.19	−0.08
AP15d	−0.19	0.16	−0.19	−0.01
Q_b	−0.14	0.12	*−0.22*	0.02
Δt	0.08	0.03	**0.27**	0.05
Event characteristics				
P	*−0.22*	**0.36**	**0.27**	**0.27**
IP10	*−0.24*	0.00	0.05	*0.25*
KE	*−0.24*	**0.32**	*0.24*	**0.31**
Q_{max}	**−0.29**	**0.29**	−0.03	**0.28**
TR	−0.17	**0.38**	−0.08	0.04
ΔQ	−0.06	0.18	**0.29**	**0.35**
RL	0.03	−0.13	0.12	*−0.23*
K	0.10	0.17	−0.03	**−0.31**
S_D	−0.04	**0.37**	0.12	−0.09
Concentrations during the event				
$C_{initial}$	−0.06	0.04	**0.40**	**−0.54**
C_{max}	0.08	0.15	0.16	*0.25*
C_{mean}	−0.14	0.08	0.16	*0.24*

AP7d is the accumulated rainfall 7 d before the event. AP15d is the accumulated rainfall 15 d before the event. Q_b is the discharge at the beginning of the event. Δt is the time elapsed from the previous runoff event. P is the rainfall amount. IP10 is the maximum 10 min rainfall intensity. KE is the rainfall kinetic energy. Q_{max} is the peak discharge. TR is the total runoff of the event. ΔQ is the magnitude of the event relative of the initial baseflow. RL is the relative length of the rising limb. K is the slope of the initial phase of the hydrograph falling limb. S_D is the runoff event duration. Δt is the time from the previous runoff event. $C_{initial}$ is the initial concentration. C_{max} is the maximum concentration. C_{mean} is the mean concentration.

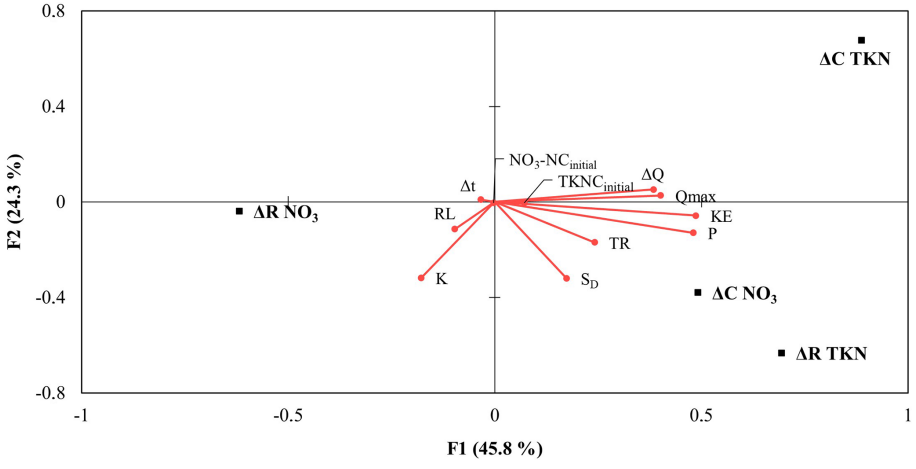

Figure 7. Redundancy analysis distance biplot showing ordinations of explanatory and response variables. The response variables (hysteresis descriptors of ΔC_{NO_3}, ΔR_{NO_3}, ΔC_{TKN}, and ΔR_{TKN}) are shown as black squares and the explanatory variables (i.e., characteristics of the events) as red circles. The red arrows are the vectors of the explanatory variables; the longer they are, the greater their influence. The first two axes of the RDA represent 45.8 % (F1) and 24.3 % (F2) of the explained variance. The angles between the response variables (hysteresis descriptors) and explanatory variables (event characteristic) reflect their correlation; the smaller the angle, the stronger the correlation. P is the rainfall amount. KE is the rainfall kinetic energy. Q_{max} is the peak discharge. TR is the total runoff of the event. ΔQ is the magnitude of the event relative to the initial baseflow. RL is the relative length of the rising limb. K is the slope of the initial phase of the hydrograph falling limb. S_D is the runoff event duration. Δt is the time from the previous runoff event. NO_3-N (or TKN) $C_{initial}$ is the initial concentration.

ning of runoff events, followed by enrichment from distal and substantial sources of nitrate, which seems not to be the case in the study catchment, because this pattern, i.e., counterclockwise with enrichment, was also observed in low-volume runoff events, so it does not seem feasible that distal sources of NO_3^- can be activated in these events. However, in large runoff events the areas of the catchment acting as nitrate sources could increase as hydrologic pathways connect, and NO_3^- also arrives from distant sources. While enrichment with counterclockwise rotation was the dominant pattern for NO_3^- in the study catchment, some events exhibited enrichment patterns but with clockwise hysteresis (Figs. 5 and 6), indicating a higher NO_3^- concentration in the rising limb of the hydrograph than in the falling limb. This pattern was mainly observed in small spring events occurring in 2008 and 2009 and could be attributed to the transport of NO_3^- from near-stream areas that have received fertilizers.

The dominance of counterclockwise nitrate hysteresis with higher concentrations on the falling limb of the hydrograph is in line with findings from reported studies conducted in forest and agricultural catchments (Butturini et al., 2006; Cerro et al., 2014; Outram et al., 2016; Musolff et al., 2021). However, they contrast with interpretations presented in several previous studies carried out in rural catchments, which only described the NO_3^- dilution processes linked to the dilution of NO_3^- concentrations in groundwater by surface runoff (Bowes et al., 2015; Aguilera and Melack, 2018; Rose et al., 2018; D'Amario et al., 2021) or the exhaustion of a finite pool of NO_3^- in the riparian zone and shallow groundwater (Koenig et al., 2017; Duncan et al., 2017). However, in the study catchment, the dilution responses (in a counterclockwise direction; $\Delta C \leq 0\,\%$) were only observed in certain larger runoff events associated with wet antecedent conditions and a short interarrival time ($\Delta t < 1$ h). A possible reason for the initial dilution of the concentrations could be the preceding wetting of the catchment, which favors the delivery of relatively low-nitrate water flushed to the stream from low NO_3^- concentration sources, such as direct rainfall; i.e., rainfall (mean NO_3^- concentrations determined in rainwater samples $= 0.1\,\mathrm{mg\,NO_3^-\,L^{-1}}$, Rodríguez-Blanco et al., 2015) falling directly into the stream or near saturated areas around the stream and runoff from roads and paved area, as has been observed in other headwater streams (Poor and McDonnell, 2007; Kato et al., 2009). Following the initial dilution, concentrations increased above pre-event values, reaching the highest NO_3^- concentrations after maximum discharge. The return of NO_3^- concentrations to the values before the rainfall–runoff event is especially slow in these cases (Fig. 5b), and NO_3^- concentrations remain elevated for several days until streamflow returns to baseflow.

Mechanisms responsible for TKN mobilization differ from those mobilizing NO_3^-. Thus, a clockwise enrichment pattern for TKN concentration was dominant for most events (Fig. 5d), suggesting a delivery of TKN to the stream network via fast pathways from proximal sources or sources relatively easily connected to the stream as the event discharge increases, with possible rapid exhaustion of the material to be transported (Creed et al., 2015). The TKN response was almost concurrent with discharge, which leads to our thinking that TKN may come from the eroded soil and litter layer, delivered to the stream primarily by surface runoff, in a similar way to the suspended sediment matter and particulate phosphorus (Rodríguez-Blanco et al., 2013, 2019). These results generally agree with many others who also reported clockwise organic nitrogen hysteresis patterns (Vanderbilt et al., 2003; Inamdar and Mitchell, 2006; Rose et al., 2018; D'Amario et al., 2021). In contrast, Hagedorn et al. (2000) observed counterclockwise hysteresis for organic nitrogen in a forest catchment in Switzerland due to its passage through the forest canopy and organic-rich topsoil. Others have attributed this pattern (counterclockwise) to distant source areas activated later in the runoff events as the hydrological pathways connect (Aguilera and Melack, 2018). In the study area, this pattern (counterclockwise) was only observed during some low-volume runoff events caused by low-rainfall events (specifically, 20 of the 26 events with this counterclockwise pattern were associated with less than 16 mm of rainfall) recorded in spring and summer, so the delivery from distant sources is less likely to explain the counterclockwise pattern due to the reduced hydrological response of these events. Rather, given the event characteristics (low-volume rainfall and runoff events with little particulate material), the presence of counterclockwise hysteresis could be indicative of a large proportion of dissolved fraction in TKN, which passes through the soil and subsequently enters the stream by subsurface flow.

Hysteresis patterns may vary among events and antecedent soil moisture conditions are often recognized as being an important factor in the response of different constituent concentrations among events, even when rainfall characteristics are approximately similar (Butturini et al., 2006; Baker and Showers, 2019). However, other authors have highlighted the important role played by rainfall–runoff events characteristic on hysteresis patterns (Chen et al., 2012; Lloyd et al., 2016). For example, Chen et al. (2012) emphasized the role of the runoff event magnitude in influencing the magnitude and direction of the hysteresis patterns, whereas Lloyd et al. (2016) underlined the combined effect exerted by storm duration, maximum discharge during the runoff event, and the time elapsing from the previous runoff events on controlling the N hysteresis magnitude and rotation. In this catchment, hysteresis direction and magnitude for TKN were better explained by the event characteristics, such as rainfall amount (P), peak discharge ($Q_{\max}$), and event magnitude relative to the initial baseflow (ΔQ) than by antecedent rainfall (AP7d and AP15d) and baseflow (Q_b). Thus, the hysteresis magnitude value was dependent on the magnitude of the hydrological response of the catchment and the delivery of particulate material to the stream. In the catchment, the main sediment supply to the stream is associated with the erosion of culti-

vated soil with high connectivity to the stream, which favors the quick delivery of particulate material to the stream. The results obtained for TKN are consistent with the findings obtained for suspended sediments, phosphorus, and particulate metals in the study area by Rodríguez-Blanco et al. (2010, 2013, 2018), showing that sources of particulate material are close to the monitoring station, which may explain the prevalence of clockwise hysteresis for TKN. For NO_3^- hysteresis patterns, the role of hydrometeorological conditions was more complex, and dynamics should be controlled by biogeochemical processes coupled with hydrological processes (Butturini et al., 2006; Heathwait e and Bieroza, 2020). For example, Heathwaite and Bieroza (2020), when analyzing the interplay between hydrological flushing and biogeochemical cycling during high- and low-magnitude events in an agricultural catchment in the UK, emphasized that the pattern of NO_3^- mobilization is controlled by the magnitude of the runoff event, with high-magnitude runoff events driving rapid mobilization (clockwise hysteresis with dilution) and low-magnitude runoff events driving delayed mobilization (counterclockwise hysteresis with enrichment). In the study catchment, the NO_3^- hysteresis magnitude (ΔC) was related to the initial NO_3 concentrations (NO_3-$NC_{initial}$), the magnitude of the event relative to the initial baseflow (ΔQ), and the time elapsed since a preceding runoff event (Δt), which highlights that, beyond the magnitude of the runoff event's essential driver for NO_3^- hysteresis magnitude variability, the inter-event period, during which physical and biological processes operate to increase the store of available nutrients and sediments (Walling and Webb, 1982), in addition to the pre-event biogeochemical conditions, also influenced the NO_3^- hysteresis magnitude (ΔC). However, this last driver does not appear to be the most relevant, indicating that initial NO_3 concentrations (NO_3-$NC_{initial}$) play a more subtle and diffuse role (Fig. 7).

5 Conclusion

Our study uses measurements of stream discharge and nitrogen (NO_3^- and TKN) obtained by intensive sampling to investigate the nitrogen concentration dynamics at the event scale. The results show the potential of high-frequency N concentration monitoring to advance our understanding of coupled hydrological and biogeochemical systems in the context of contrasting hydrometeorological conditions. An assessment of nitrogen C–Q relationships and their controlling factors has provided evidence of the different NO_3^- and TKN dynamics during the runoff events, suggesting the presence of distinct delivery mechanisms and differences in dominant hydrological pathways. NO_3^- behavior during the runoff events was dominated by counterclockwise hysteresis, whereas clockwise hysteresis prevailed in the TKN dynamic. However, for both solutes (NO_3^- and TKN), the magnitude of the hydrological response played a primary role in controlling the magnitude of hysteresis variability.

The divergence dynamics observed between N components in the study area highlights the need to understand the transportation of N and the mechanism for controlling the implementation of future water quality monitoring programs and the development of N-specific management plans to ensure that control measures are most effective at the catchment scale, especially within the context of increasing nitrate concentrations, which is a pressing environment issue. Thus, to minimize nitrate delivery to streams, catchment management should focus on reducing N stores in the soil, whereas, for protecting water quality against TKN, management options to reduce surface runoff and sediment are also required, since they seem to be mainly responsible for TKN transport in this region.

Data availability. The data that support the findings of this study are available from the corresponding author upon reasonable request.

Author contributions. The original draft of the paper was prepared by MLRB, and reviewing and editing were done by MTTC and MMTC. All authors have read and agreed to the current version of the paper.

Competing interests. The contact author has declared that none of the authors has any competing interests.

Disclaimer. Publisher's note: Copernicus Publications remains neutral with regard to jurisdictional claims in published maps and institutional affiliations.

Acknowledgements. We would like to thank the two anonymous reviewers for their helpful comments and suggestions.

Financial support. This research has been supported by the Spanish Ministry of Education and Science (grant no. REN2003-08143) and Xunta of Galicia (grant nos. PGIDIT05RAG10303PR and 10MDS103031PR).

Review statement. This paper was edited by Roger Moussa and reviewed by two anonymous referees.

References

Aguilera, R. and Melack, J. M.: Concentration-discharge responses to storm events in Coastal California Watersheds, Water Resour.

Res., 54, 407–424, https://doi.org/10.1002/2017WR021578, 2018.

Ameijenda, C.: Integrated management of water resources and its application to local planning of the Abegondo Cecebre 07/ENV/E/0826 LIFE+project, Span. J. Rural Develop., 1, 35–40, https://doi.org/10.5261/2010.ESP1.02, 2010.

APHA: Standard Methods for Examination of Water and Wastewater, APHA, Washington, ISBN 0875532357, 1998.

Baker, E. B. and Showers, W. J.: Hysteresis analysis of nitrate dynamics in the Neuse River, NC, 652, Sci. Total Environ., 652, 889–899, https://doi.org/10.1016/j.scitotenv.2018.10.254, 2019.

Bernal, S., Butturini, A., and Sabater, F.: Seasonal variations of dissolved nitrogen and DOC : DON ratios in an intermittent Mediterranean stream, Biogeochemistry, 75, 351–372, https://doi.org/10.1007/s10533-005-1246-7, 2005.

Bieroza, M. Z. and Heathwaite, A. L.: Seasonal variation in phosphorus concentration-discharge hysteresis inferred from high-frequency in situ monitoring, J. Hydrol., 524, 333–347, https://doi.org/10.1016/j.jhydrol.2015.02.036, 2015.

Bieroza, M. Z., Heathwaite, A. L., Bechmann, M., Kyllmar, K., and Jordan, P.: The concentration-discharge slope as a tool for water quality management, Sci. Total Environ., 630, 738–749, https://doi.org/10.1016/J.SCITOTENV.2018.02.256, 2018.

Bowes, M. J., Jarvie, H. P., Halliday, S. J., Skeffington, R. A., Wade, A. J., Loewenthal, M., Gozzard, E., Newman, J. R., and Palmer-Felgate, E. J.: Characterising phosphorus and nitrate inputs to a rural river using high-frequency concentration-flow relationships, Sci. Total Environ., 511, 889–899, https://doi.org/10.1016/j.scitotenv.2014.12.086, 2015.

Butturini, A., Francesc, G., Jérôme, L., Eusebi, V., and Francesc, S.: Cross-site comparison of variability of DOC and nitrate c–q hysteresis during the autumn-winter period in three Mediterranean headwater streams: A synthetic approach, Biogeochemistry, 77, 327–349, https://doi.org/10.1007/s10533-005-0711-7, 2006.

Butturini, A., Alvarez, M., Bernał, S., Vazquez, E., and Sabater, F.: Diversity and temporal sequences of forms of DOC and NO_3^- discharge responses in an intermittent stream: Predictable or random succession?, J. Geophys. Res.-Biogeo., 113, G03016, https://doi.org/10.1029/2008JG000721, 2008.

Camargo, J. A. and Alonso, A.: Contaminación por nitrógeno inorgánico en los ecosistemas acuáticos: problemas medioambientales, criterios de calidad del agua, e implicaciones del cambio climático, Ecosistemas, 16, 98–110, 2007.

Cerro, I., Sanchez-Perez, J. M., Ruiz-Romera, E., and Antigüedad, I.: Variability of particulate (SS, POC) and dissolved (DOC, NO_3) matter during storm events in the alegria agricultural watershed, Hydrol. Process., 28, 2855–2867, https://doi.org/10.1002/hyp.9850, 2014.

Chen, N., Wu, J., and Hong, H.: Effect of storm events on riverine nitrogen dynamics in a subtropical watershed, southeastern China, Sci. Total Environ., 431, 357–365, https://doi.org/10.1016/j.scitotenv.2012.05.072, 2012.

Creed, I. F., Mcknight, D. D. M., Pellerin, B. A., Green, M. B., Bergamaschi, B. A., and Aiken, G. R.: The river as a chemostat: Fresh perspectives on dissolved organic matter flowing down the river continuum, Can. J. Fish. Aquat. Sci., 14, 1272–1285, https://doi.org/10.1139/cjfas-2014-0400, 2015.

D'Amario, S. C., Wilson, H. F., and Xenopoulos, M. A.: Concentration-discharge relationships derived from a larger regional dataset as a tool for watershed management, Ecol. Appl., 31, e02447, https://doi.org/10.1002/eap.2447, 2021.

de Barros, C. A. P., Tiecher, T., Ramon, R., dos Santos, D. R., Bender, M. A., Evrard, O., Ayrault, S., and Minella, J. P. G.: Investigating the relationships between chemical element concentrations and discharge to improve our understanding of their transport patterns in rural catchments under subtropical climate conditions, Sci. Total Environ., 748, 141345, https://doi.org/10.1016/J.SCITOTENV.2020.141345, 2020.

Duncan, J. M., Band, L. E., and Groffman, P. M.: Variable nitrate concentration–discharge relationships in a forested watershed, Hydrol. Process., 31, 1817–1824, https://doi.org/10.1002/HYP.11136, 2017.

Dunkerley, D.: Rain event properties in nature and in rainfall simulation experiments: A comparative review with recommendations for increasingly systematic study and reporting, Hydrol. Process., 22, 4415–4435, https://doi.org/10.1002/HYP.7045, 2008.

Dupas, R., Jomaa, S., Musolff, A., Borchardt, D., and Rode, M.: Disentangling the influence of hydroclimatic patterns and agricultural management on river nitrate dynamics from sub-hourly to decadal time scales, Sci. Total Environ., 571, 791–800, https://doi.org/10.1016/j.scitotenv.2016.07.053, 2016.

EC (European Comision): Informe de la comisión al parlamento europeo y al consejo sobre la aplicación de la directiva marco sobre el agua (2000/60/CE) y la directiva sobre inundaciones (2007/60/CE) segundos planes hidrológicos de cuenca primeros planes de gestión del riesgo de inundación, SWD 42, 234 pp., 2019.

EEA: European waters – Assessment of status and pressures 2018, 90 pp., 2018.

Eludoyin, A. O., Griffith, B., Orr, R. J., Bol, R., Quine, T. A., and Brazier, R. E.: An evaluation of the hysteresis in chemical concentration–discharge (C–Q) relationships from drained, intensively managed grasslands in southwest England, Hydrolog. Sci. J., 62, 1243–1254, https://doi.org/10.1080/02626667.2017.1313979, 2017.

EU (European Union): Directive 98/83/CE relative to human drinking water quality, Official Journal of European Communities L330, 1998.

EU (European Union): Directive 2000/60/CE of the European Parliament and of the Council establishing a framework for community action in the field of water policy, Official Journal of European Communities L327, 2000.

Evans, C. and Davies, T. D.: Causes of concentration/discharge hysteresis and its potential as a tool for analysis of episode hydrochemistry, Water Resour. Res., 34, 129–137, https://doi.org/10.1029/97WR01881, 1998.

Fovet, O., Humbert, G., Dupas, R., Gascuel-Odoux, C., Gruau, G., Jaffrézic, A., Thelusma, G., Faucheux, M., Gilliet, N., and Hamon, Y.: Seasonal variability of stream water quality response to storm events captured using high-frequency and multi-parameter data, J. Hydrol., 559, 282–293, https://doi.org/10.1016/j.jhydrol.2018.02.040, 2018.

García-Ruiz, J. M., Arnáez, J., Beguería, S., Seeger, M., Martí-Bono, C., Regüés, D., Lana-Renault, N., and White, S.: Runoff generation in an intensively disturbed, abandoned farmland catchment, Central Spanish Pyrenees, Catena, 59, 79–92, https://doi.org/10.1016/j.catena.2004.05.006, 2005.

Hagedorn, F., Schleppi, P., Waldner, P., and Flühler, H.: Export of dissolved organic carbon and nitrogen from Gleysol dominated catchments – The significance of water flow paths, Biogeochemistry, 50, 129–137, https://doi.org/10.1023/A:1006398105953, 2000.

Heathwaite, A. L. and Bieroza, M.: Fingerprinting hydrological and biogeochemical drivers of freshwater quality, 137–161, https://doi.org/10.1002/hyp.13973, 2020.

Hewlett, J. D. and Hibbert, A. R.: Factors Affecting the Response of Small Watersheds to Precipitation in Humid Areas, in: Proceedings of the International Symposium on Forest Hydrology, edited by: Sopper, W. E. and Lull, H. W., Pergamon, Pennsylvania State University, New York, 275–290, 1967.

IGME (Instituto Tecnológico Geominero de España): Mapa Geológico de España, 1 : 50000, Hoja 45, Betanzos, Spain, 1981.

Inamdar, S. P. and Mitchell, M. J.: Hydrologic and topographic controls on storm-event exports of dissolved organic carbon (BOC) and nitrate across catchment scales, Water Resour. Res., 42, W034321, https://doi.org/10.1029/2005WR004212, 2006.

Instituto Geográfico Nacional: Atlas nacional de España 1986–2006, Centro Nacional de Información Geográfica, Madrid, 2008.

IUSS Working Group WRB: World Reference Base for Soil Resources 2014, International soil classification system for naming soils and creating legends for soil maps, World Soil Resources Reports, no. 106, FAO, Rome, 2015.

Kato, T., Kuroda, H., and Nakasone, H.: Runoff characteristics of nutrients from an agricultural watershed with intensive livestock production, J. Hydrol., 368, 79–87, https://doi.org/10.1016/j.jhydrol.2009.01.028, 2009.

Kaushal, S. S. and Lewis, W. M.: Patterns in the chemical fractionation of organic nitrogen in Rocky Mountain streams, Ecosystems, 6, 483–492, https://doi.org/10.1007/s10021-003-0175-3, 2003.

Knapp, J. L. A., von Freyberg, J., Studer, B., Kiewiet, L., and Kirchner, J. W.: Concentration–discharge relationships vary among hydrological events, reflecting differences in event characteristics, Hydrol. Earth Syst. Sci., 24, 2561–2576, https://doi.org/10.5194/hess-24-2561-2020, 2020.

Koenig, L. E., Shattuck, M. D., Snyder, L. E., Potter, J. D., and McDowell, W. H.: Deconstructing the Effects of Flow on DOC, Nitrate, and Major Ion Interactions Using a High-Frequency Aquatic Sensor Network, Water Resour. Res., 53, 10655–10673, https://doi.org/10.1002/2017WR020739, 2017.

Latron, J., Soler, M., Llorens, P., and Gallart, F.: Spatial and temporal variability of the hydrological response in a small Mediterranean research catchment (Vallcebre, Eastern Pyrenees), Hydrol. Process., 22, 775–787, https://doi.org/10.1002/HYP.6648, 2008.

Legendre, P. and Legendre, L.: Numerical Ecology, Elsevier, Amsterdam, the Netherlands, 1998.

Linsley, R. K., Kohler, M. A., and Paulhus, J. C.: Applied Hydrology, McGraw-Hill Book Co., New York, p. 689, 1949.

Lloyd, C. E. M., Freer, J. E., Johnes, P. J., and Collins, A. L.: Using hysteresis analysis of high-resolution water quality monitoring data, including uncertainty, to infer controls on nutrient and sediment transfer in catchments, Sci. Total Environ., 543, 0444892508, https://doi.org/10.1016/j.scitotenv.2015.11.028, 2016.

López Periago, E., Núnez Delgado, A., and Díaz-Fierros, F.: Attenuation of groundwater contamination caused by cattle slurry: a plot-scale experimental study, Bioresource Technol., 84, 105–111, https://doi.org/10.1016/S0960-8524(02)00041-X, 2002.

Lorite-Herrera, M., Hiscock, K., and Jiménez-Espinosa, R.: Distribution of dissolved inorganic and organic nitrogen in river water and groundwater in an agriculturally-dominated catchment, south-East Spain, Water Air Soil Poll., 198, 335–346, https://doi.org/10.1007/s11270-008-9849-y, 2009.

Musolff, A., Zhan, Q., Dupas, R., Minaudo, C., Fleckenstein, J. H., Rode, M., Dehaspe, J., and Rinke, K.: Spatial and Temporal Variability in Concentration-Discharge Relationships at the Event Scale, Water Resour. Res., 57, e2020WR029442, https://doi.org/10.1029/2020WR029442, 2021.

Outram, F. N., Cooper, R. J., Sünnenberg, G., Hiscock, K. M., and Lovett, A. A.: Antecedent conditions, hydrological connectivity and anthropogenic inputs: Factors affecting nitrate and phosphorus transfers to agricultural headwater streams, Sci. Total Environ., 545–546, 184–199, https://doi.org/10.1016/j.scitotenv.2015.12.025, 2016.

Palleiro, L., Rodríguez-Blanco, M. L., Taboada-Castro, M. M., and Taboada-Castro, M. T.: Hydrological response of a humid agroforestry catchment at different time scales, Hydrol. Process., 28, 1677–1688, https://doi.org/10.1002/hyp.9714, 2014.

Poor, C. J. and McDonnell, J. J.: The effects of land use on stream nitrate dynamics, J. Hydrol., 332, 54–68, https://doi.org/10.1016/j.jhydrol.2006.06.022, 2007.

Ramos, T. B., Gonçalves, M. C., Branco, M. A., Brito, D., Rodrigues, S., Sánchez-Pérez, J. M., Sauvage, S., Prazeres, Â., Martins, J. C., Fernandes, M. L., and Pires, F. P.: Sediment and nutrient dynamics during storm events in the Enxoé temporary river, southern Portugal, Catena, 127, 177–190, https://doi.org/10.1016/j.catena.2015.01.001, 2015.

Rodríguez-Blanco, M. L.: Estudio integrado de los procesos de escorrentía y exportación de sedimentos y fósforo en una cuenca rural, Doctoral dissertation, 2009.

Rodríguez-Blanco, M. L., Taboada-Castro, M. M., and Taboada-Castro, M. T.: Factors controlling hydro-sedimentary response during runoff events in a rural catchment in the humid Spanish zone, Catena, 82, 206–217, https://doi.org/10.1016/j.catena.2010.06.007, 2010.

Rodríguez-Blanco, M. L., Taboada-Castro, M. M., and Taboada-Castro, M. T.: Rainfall-runoff response and event-based runoff coefficients in a humid area (northwest Spain), Hydrolog. Sci. J., 57, 445–459, https://doi.org/10.1080/02626667.2012.666351, 2012.

Rodríguez-Blanco, M. L., Taboada-Castro, M. M., and Taboada-Castro, M. T.: Phosphorus transport into a stream draining from a mixed land use catchment in Galicia (NW Spain): Significance of runoff events, J. Hydrol., 481, 12–21, https://doi.org/10.1016/j.jhydrol.2012.11.046, 2013.

Rodríguez-Blanco, M. L., Taboada-Castro, M. M., Taboada-Castro, M. T., and Oropeza-Mota, J. L.: Relating nitrogen export patterns from a mixed land use catchment in NW Spain with rainfall and streamflow, Hydrol. Process., 29, 2720–2730, https://doi.org/10.1002/hyp.10388, 2015.

Rodríguez-Blanco, M. L., Soto-Varela, F., Taboada-Castro, M. M., and Taboada-Castro, M. T.: Using hysteresis analysis to infer controls on sediment-associated and dissolved metals transport

in a small humid temperate catchment, J. Hydrol., 565, 49–60, https://doi.org/10.1016/j.jhydrol.2018.08.030, 2018.

Rodríguez-Blanco, M. L., Taboada-Castro, M. M., and Taboada-Castro, M. T.: An overview of patterns and dynamics of suspended sediment transport in an agroforest headwater system in humid climate: Results from a long-term monitoring, Sci. Total Environ., 648, 33–43, https://doi.org/10.1016/j.scitotenv.2018.08.118, 2019.

Rodríguez-Blanco, M. L., Taboada-Castro, M. M., and Taboada-Castro, M. T.: An assessment of the recent evolution of the streamflow in a near-natural system: A case study in the headwaters of the mero basin (Galicia, Spain), Hydrology, 7, 97, https://doi.org/10.3390/hydrology7040097, 2020.

Rose, L. A., Karwan, D. L., and Godsey, S. E.: Concentration–discharge relationships describe solute and sediment mobilization, reaction, and transport at event and longer timescales, Hydrol. Process., 32, 2829–2844, https://doi.org/10.1002/hyp.13235, 2018.

Singh, V. P.: Hydrologic Systems. Rainfall-runoff Modelling, Prentice Hall, New Jersey, EEUU, 1988.

Taboada-Castro, M. M., Lado, M., Diéguez Villar, A., and Paz González, A.: Evolución temporal de la infiltración superficial a escala de parcela, in: Avances Sobre el Estudio de la Erosión Hídrica, edited by: Paz, A. and Taboada, M. T., Universidade da Coruña, A Coruña, Spain, ISBN 84-89694-34-6, 1999.

Tardy, Y.: Le cycle de léau. climats, paléoclimasts et géochimie globale, Mason, Paris, 1986.

Vanderbilt, K. L., Lajtha, K., and Swanson, F. J.: Biogeochemistry of unpolluted forested watersheds in the Oregon Cascades: Temporal patterns of precipitation and stream nitrogen fluxes, Biogeochemistry, 62, 87–117, https://doi.org/10.1023/A:1021171016945, 2003.

Vaughan, M. C. H., Bowden, W. B., Shanley, J. B., Vermilyea, A., Sleeper, R., Gold, A. J., Pradhanang, S. M., Inamdar, S. P., Levia, D. F., Andres, A. S., Birgand, F., and Schroth, A. W.: High-frequency dissolved organic carbon and nitrate measurements reveal differences in storm hysteresis and loading in relation to land cover and seasonality, Water Resour. Res., 53, 5345–5363, https://doi.org/10.1002/2017WR020491, 2017.

Walling, D. E. and Webb, B. W.: Sediment availability and the prediction of storm-period sediment yields, Recent developments in the explanation and prediction of erosion and sediment yield, 137, 327–337, 1982.

Williams, G. P.: Sediment concentration versus water discharge during single hydrologic events in rivers, J. Hydrol., 111, 89–106, https://doi.org/10.1016/0022-1694(89)90254-0, 1989.

Winter, C., Lutz, S. R., Musolff, A., Kumar, R., Weber, M., and Fleckenstein, J. H.: Disentangling the Impact of Catchment Heterogeneity on nitrate export dynamics from event to long-term time scales, Water Resour. Res., 57, https://doi.org/10.1029/2020WR027992, 2021.

Wischmeier, W. H. and Smith, D. D.: Rain fall energy and its relationship to soil loss, EOS T. Am. Geophys. Un., 39, 285–291, 1958.